# RECENT DEVELOPMENTS IN THE NONLINEAR ANALYSIS OF REINFORCED CONCRETE STRUCTURES USING THREE DIMENSIONAL FINITE ELEMENT MODELS

M. Cervera, E. Hinton and O. Hassan

University College of Swansea

SUMMARY

In this paper we review our efforts to develop an efficient and accurate 3D finite element model which can be used in the nonlinear analysis of reinforced concrete structures with particular emphasis on plates and shells. The need for good pre- and post-processing facilities is also highlighted.

## 1. INTRODUCTION

Computer-aided structural analysis of reinforced concrete structures has been the object of extensive research for almost twenty years. Attention first focused on two-dimensional and axisymmetric models, but it was soon widened to include plate and shell systems. Problems involving reinforced concrete shells are of great practical interest, as they include those that appear in nuclear engineering, gas storage tanks, etc.

The usual method of modelling reinforced concrete shell structures is to make use of the so-called 'layered' shell elements. The elements are composed of a series of through-thickness 'layers', each assumed to be in a state of plane stress. This approach has several disadvantages:

(a) The quadrature rule used to integrate quantities such as the residual forces and the tangential stiffness through the thickness (i.e. the mid-ordinate rule) is not very accurate, and many layers (eight to twelve) must be used to ensure reasonable accuracy.

(b) The large number of sampling points used per element makes the evaluation of the tangential stiffness matrix and internal force vector quite expensive.

(c) The plane stress assumption in the layered plate or shell implies that the normal stress perpendicular to the midsurface is neglected. Furthermore, in most models, in-plane stresses are treated separately from transverse shear stresses, usually in an inconsistent way.

(d) Cracks are assumed to form due to in-plane stresses only, the effect of the transverse shear stresses being disregarded when checking for cracking. As a result, cracks are perpendicular to the midsurface, which is an unrealistic constraint of the model that makes it unable to represent non-flexural failures.

(e) The elements used are usually of the Mindlin-type. This results in an 'a priori' imposed uniform distribution of transverse shear strains through the thickness.

(f) Concrete slabs are usually moderately thick, so consideration of transverse shear strains and stresses is not insignificant, especially near the supports.

All these considerations point to the necessity of developing fully three dimensional models which can be used to analyse reinforced concrete structures both efficiently and accurately.

The use of a standard three dimensional approach for the analysis avoids the complexities associated with shell formulations, allows for a wider range of applications, and is free from the simplifying assumptions mentioned above. On the other hand, a 3D analysis usually involves a larger number of degrees of freedom for a given discretization than a shell formulation, and requires better mesh-generation and post-processing facilities than those of an essentially two dimensional analysis.

This paper reviews our efforts to develop such a 3D model for nonlinear structural analysis of reinforced concrete structures subjected to short term static loading.

## 2. THREE DIMENSIONAL COMPUTATIONAL MODEL

The three dimensional computational model is now described. Firstly, the finite element discretization is discussed with particular attention given to the type of integration rule adopted and problems of locking behaviour. Next, the constitutive models adopted are presented. Thirdly, the nonlinear equation solution procedures are considered. Finally, the need for careful pre- and post- processing of the data in three-dimensional analysis is emphasised.

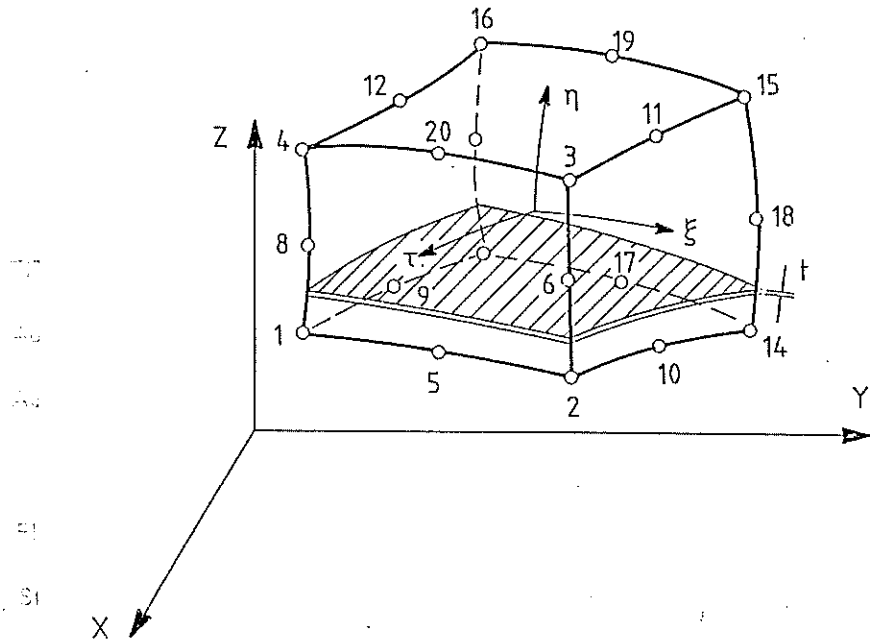


Figure 1. 20-noded isoparametric solid element with reinforcement

## 2.2 Finite element model

(a) Concrete solid. The 20-node isoparametric element shown in Figure 1 is used in this work. Hierarchical, rather than standard, interpolation functions [1] are used in the present formulation. Trilinear shape functions are used for the eight corner nodes and quadratic hierarchical shape functions are employed for the twelve mid-side nodes. The use of this hierarchical approach provides a 'natural' preconditioning matrix when iterative solution techniques (such as the conjugate gradient method) are used. Furthermore, hierarchically derived stiffness matrices are better conditioned than the standard ones. This feature is of additional advantage when analysing plates and shells with three-dimensional elements.

To evaluate the necessary volume integrals which occur in the stffness matrix and residual force vector numerical integration is used. A fifteen point rule [2] is employed. The location of the sampling points is shown in Figure 2. This particular rule is chosen because it requires less computational time than the usual 3x3x3 Gaussian rule, and unlike the reduced 2x2x2 Gauss rule it does not produce any spurious mechanism.

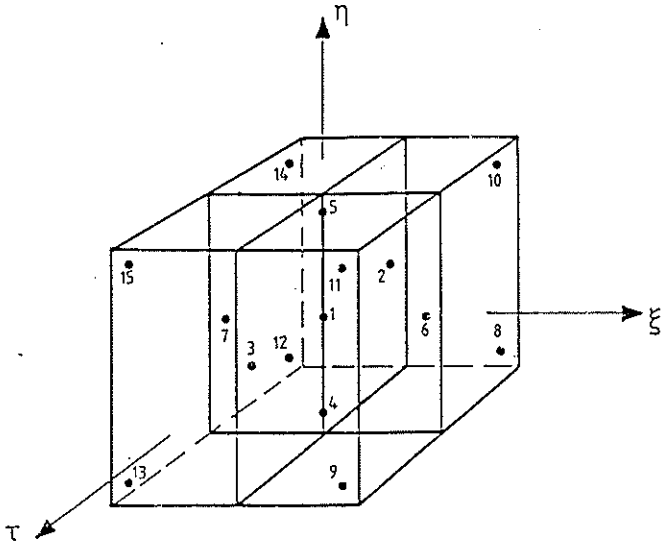


Figure 2. Distribution of the integration points

As the solid finite element is intended for use in the analysis of plates and shells of various thicknesses, some linear elastic aspect ratio tests were carried out. A series of uniformely-loaded square plates of various span-to-thickness ratios, a/h, were analysed with two sets of boundary conditions: (i) simply supported on all edges, and (ii) clamped conditions on all edges.

Figure 3 shows results for the two analyses using a 4x4x1 mesh. As expected, a shear locking type behaviour is observed for thin situations.

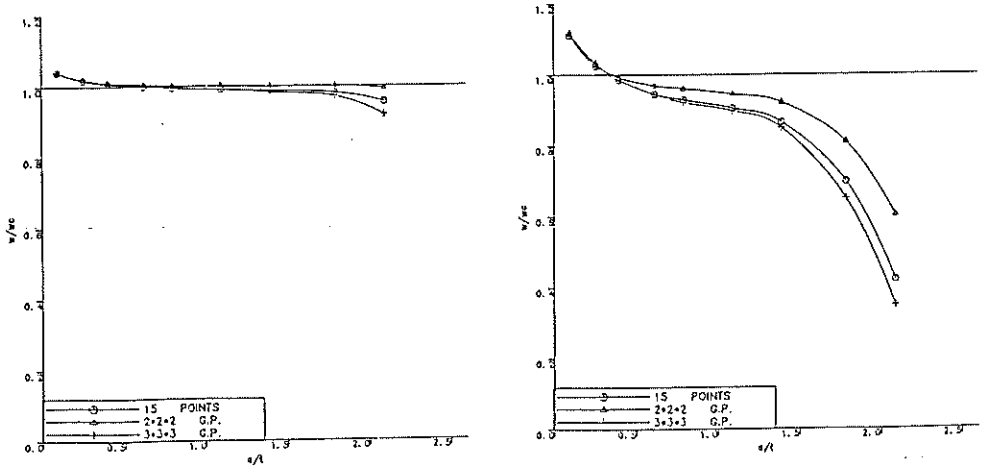


Figure 3. Aspect ratio tests

(a) simply-supported plate; (b) clamped plate.

From a careful analysis of these and other results it appears wise to limit the aspect ratio of individual 20-node brick elements to a maximum of about 25 when bending action predominates and when adequate computational precision (at least 11 significant digits) is available.

Other quadratic solid elements are currently being investigated to extend the range of applicability of the 3D model.

(b) Reinforcing steel. Perfect bond is assumed between the steel reinforcement and the surrounding concrete. The assumption of compatibility of displacements and strains between concrete and steel allows the steel to be treated as part of the 3D element. The steel stiffness and resisting forces are added to those of the concrete to obtain the global quantities of the element.

Each set of reinforcing bars is smeared as a two-dimensional membrane 'layer' of equivalent thickness, placed inside the element as shown in Figure 1. The steel is assumed to possess uniaxial material properties. The angle between the local tangent at each sampling point of the steel membrane and the local coordinate system may be arbitrary. This treatment for the steel is identical to the procedure used for 'layered elements' usually employed for plates and shells.

## 2.2 Concrete constitutive model

The constitutive models employed here account for various types of material nonlinearities in the concrete and steel. The material behaviour is assumed to be independent of time.

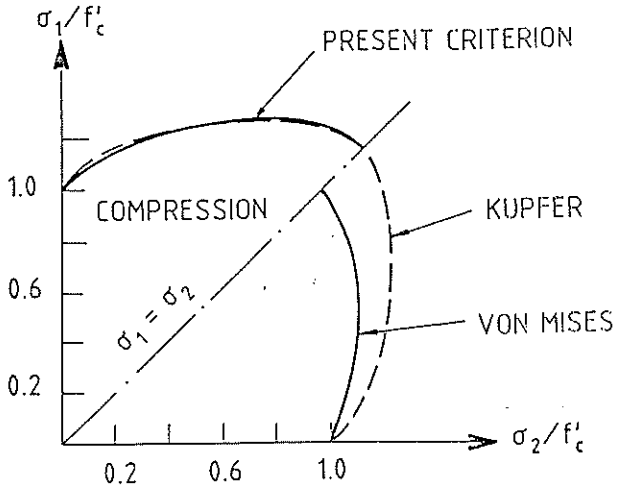


Figure 4. Present yield surface

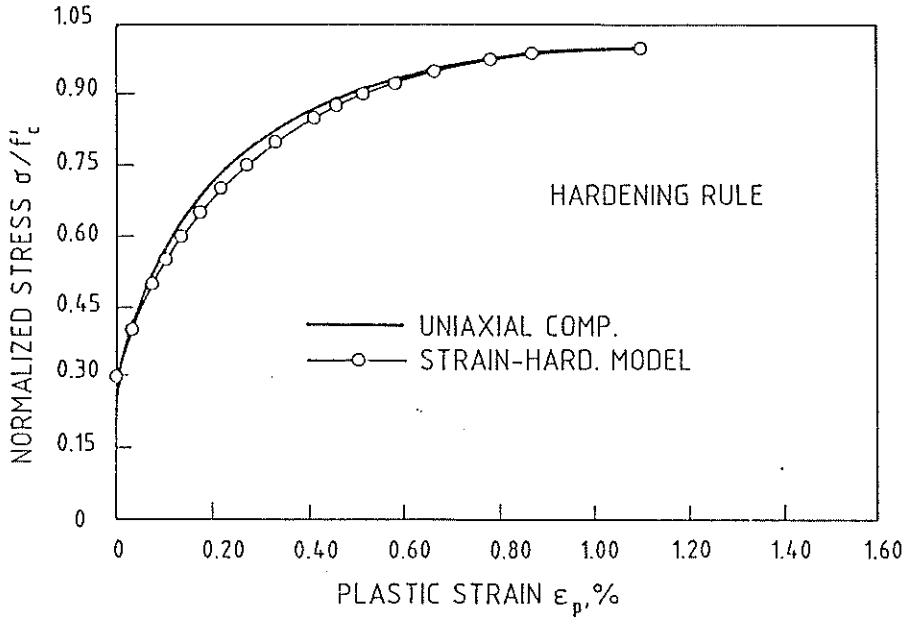


Figure 5. Hardening rule.

(a) Uncracked concrete. Experimental evidence indicates that the stress-strain relationship for concrete is non-linear even for low stress levels. The inelastic deformation may be separated into recoverable and irrecoverable components. In the present model, elasticity is used for the recoverable strain components, and a work-hardening associated plasticity approach is employed to model the irrecoverable part of the deformation.

The yield function selected depends on the first two stress invariants [3] and can be written as

$$f(I_1,J_2) = [\ \alpha I_1 + 3\beta J_2\ ]^{1/2} = \sigma_o \qquad (1)$$

The values $\alpha = 0.355$ and $\beta = 1.355$ are suggested for and adequate fitting to experimental data [4] (see Figure 4).

A value of $\sigma_o = \alpha_1 f'$ (being 0.3 a typical value for $\alpha_1$) defines a surface limiting the elastic behaviour. When this surface is reached inelastic deformation begins and a hardening rule monitors the expansion of the yield surface under further loading. In this way, a family of 'loading surfaces' is defined. The hardening rule chosen is the conventional 'Madrid Parabola', which can be expressed as

$$\sigma_o = -E_o\varepsilon_p + (\ 2E_o^2\varepsilon_o\varepsilon_p\ )^{1/2} \qquad \alpha_1 f'_c \leq \sigma_o \leq f'_c \qquad (2)$$

where $\alpha_o$ is the effective sress, $E_o$ is the initial Young's modulus, $\varepsilon_o$ is the total strain at peak stress and $\varepsilon$ is the plastic strain. Values $\alpha_1 = 0.3$ and $\varepsilon_o = 2f'_c/E_o$ provide good approximation to experimental data [4] (see Figure 5).

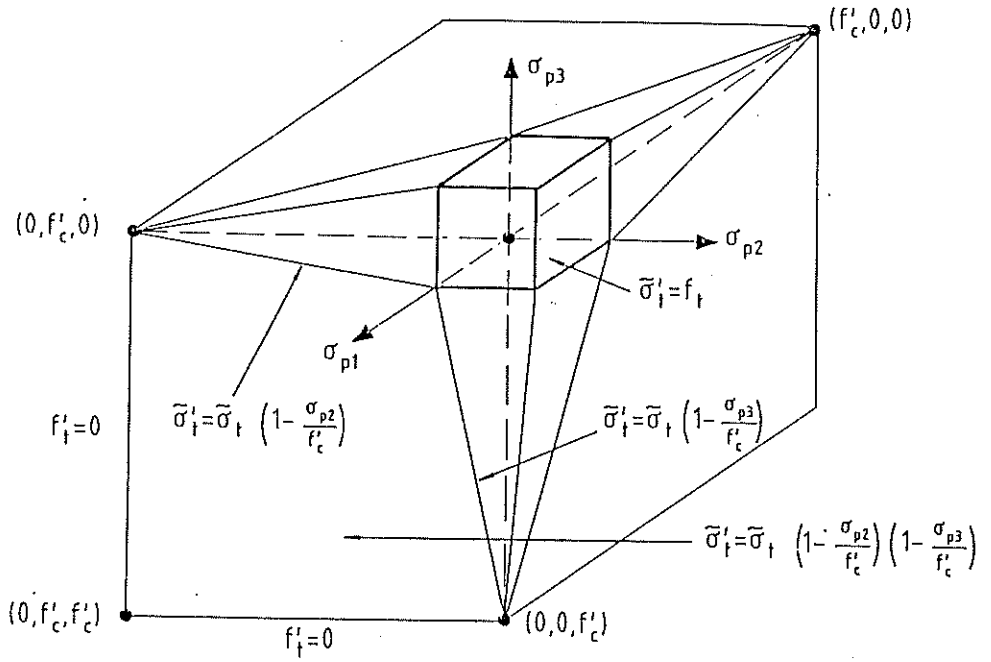


Figure 6. Cracking surfaces in stress space.

Crushing of concete is assumed to occur when a certain failure surface in the principal strain space is reached. The failure surface may be defined as

$$3\beta J_2' = \varepsilon_u^2 \tag{3}$$

where $J_2'$ is the second deviatoric strain invariant and $\varepsilon_u$ is an ultimate total strain value extrapolated from uniaxial tests (typically $\varepsilon_u$=0.003-0.004).

(b) Crack modelling. The smeared crack approach is used to model cracking. The maximum stress criterion is used: if the maximum principal stress exceeds a limiting value then a crack is formed in a plane orthogonal to the offending stress. Thereafter, concrete becomes orthotropic, with local material axes orthogonal to the crack planes. A maximum of two sets of orthogonal cracks are allowed to open at each sampling point. The limiting value required to define the onset of cracking is established as follows,

(i) in the triaxial tension zone

$$\sigma_{io} = f'_t \qquad i = 1,2,3 \tag{4}$$

as there is experimental evidence that triaxial tensile strength of concrete is almost independent of the stress ratio.

(ii) for tension-tension-compression and tension-compression-compression stress states, linearily decreasing tensile strength expressions are used,

$$\sigma_{io} = f'_t \left( 1 + \frac{\sigma_{i+1}}{f'_c} \right) \qquad \sigma_{i+1} \leq 0 \tag{5}$$

$$\sigma_{io} = f'_t \left( 1 + \frac{\sigma_{i+1}}{f'_c} \right)\left( 1 + \frac{\sigma_{i+2}}{f'_c} \right) \qquad \sigma_{i+1}, \sigma_{i+2} \leq 0 \tag{6}$$

These expressions incorporate the fact that compression in one direction favours microcracking in the orthogonal directions, thus reducing tensile capacity.

The resulting cracking surfaces are shown in Figure 6.

After cracking, the tensile stress normal to the crack is released following the exponential curve

$$\sigma = f'_t \left[ \exp\left[ -(\varepsilon - \varepsilon_o)/\alpha \right] \right] \tag{7}$$

where $f'_t$ is the concrete tensile strenght, $\varepsilon$ is the tensile strain across the crack, and $\varepsilon_o = f'_t/E_o$. The softening parameter $\alpha$ is chosen to be

$$\alpha = G_f/f'_t \, l_c \tag{8}$$

where $G_f$ is the fracture energy of concrete (assumed to be a material property) and $l_c$ is a characteristic length associated with the sampling point. The dependence of the softening branch on the size of the element implies that the cracking model is mesh independent [5].

The shear modulus is also modified for cracked concrete. The process consists of assingning to the shear modulus corresponding to the crack plane a reduced value $G_c$ defined as

$$G_c = \beta G_o \tag{9}$$

where $G_o$ is the shear modulus of uncracked concrete and $\beta$ is a reducing value in the range of zero to one. A constant value for the reducing factor has been used in many analysis. However, it is more realistic to relate the value of $\beta$ to the tensile strain normal to the crack plane, a smeared measure of the crack width. In this work, the following value is used [6]

$$\beta = 1 - \left( \varepsilon_t/0.005 \right)^{k_1} \tag{10}$$

where $\varepsilon_t$ is the tensile strain normal to the crack plane, and
$k_1$ is a parameter in the range of 0.3 to 1.0

(c) Compressive behaviour of cracked concrete

When establishing the limiting values required to define the onset of cracking, the fact that compressive stresses in the transverse directions reduce the tensile strength of concrete was taken into account in the cracking criterion. The reciprocal effect can also be accounted for: tensile strains in the crack direction effectively reduce the compressive strength in the transverse directions. This effect is included in the present model by scaling the hardening rule described earlier by a reducing factor [6]

$$\lambda = 1 - k_2 \left( \varepsilon_t / 0.005 \right) \qquad (11)$$

where $\varepsilon_t$ is the tensile stress normal to the crack plane and $k_2$ is a factor in the range of 0.1 to 0.5.

The modified hardening rule is defined by the expression

$$\sigma_o = -E_o \varepsilon_p + \left(2E_o^2 \lambda \varepsilon_o \varepsilon_p\right)^{1/2} \qquad \lambda \alpha_1 f_c' \leq \sigma_o \leq \lambda f_c' \qquad (12)$$

Comparisons of the numerical prediction and experimental results for different stress combinations are shown in Figure 7.

## 2.3 Steel reinforcement model

The steel reinforcement is assumed to have uniaxial properties in the direction of the bars. A plasticity formulation is adopted in which linear isotropic hardening is employed after initial yielding. Unloading occurs elastically.

## 2.4 Nonlinear equation solution techniques

In order to trace the entire response of the structure, an incremental/iterative technique must be adopted. Traditionally modified versions of the Newton-Raphson method have been used, thus avoiding frequent calculations and factorisations of the tangential stiffness matrix. Refinements of such techniques involving automatic load incrementation, methods for tracing the equilibrium path by updating the load level during the iterative process (i.e. arc-length and displacement control methods, and particularly, the use of inexact line searches have been found to be invaluable. A description of the application of these techniques to the analysis of reinforced concrete structures is given elsewhere [7].

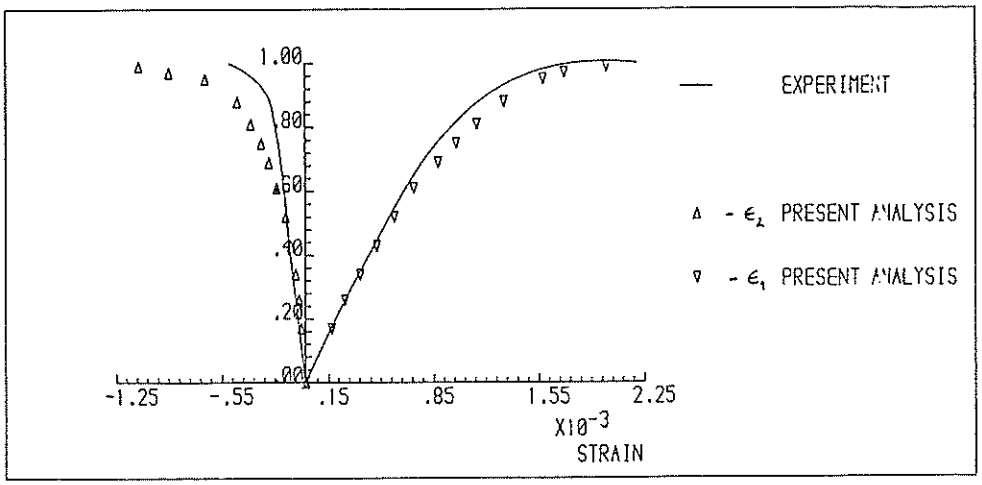


STRAIN-LOAD CURVE FOR UNIAXIAL LOAD

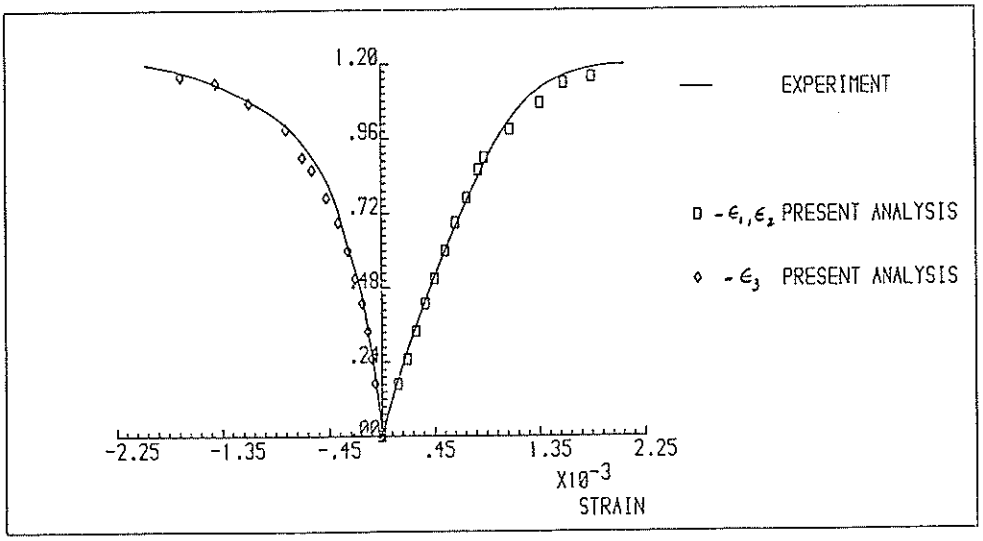


STRAIN-LOAD CURVES FOR BIAXIAL COMPRESSION

RATIO OF -1/-1

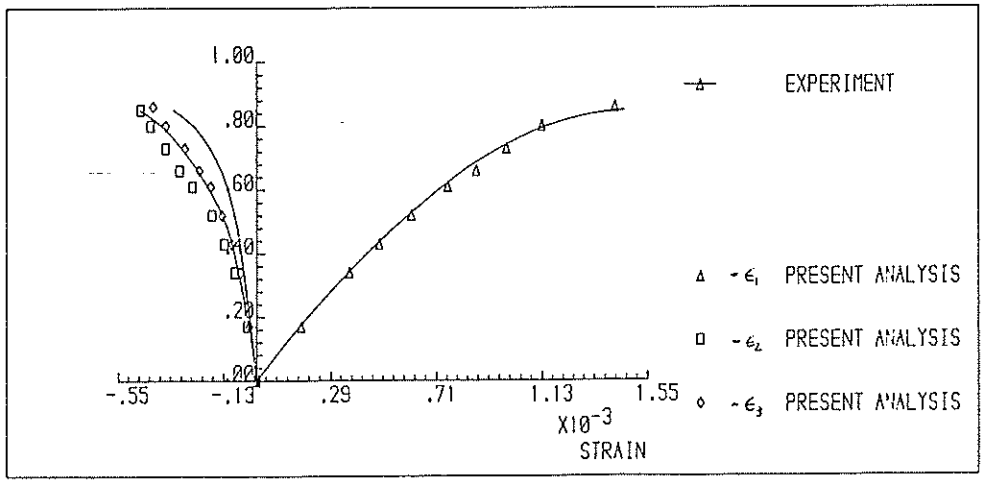


STRAIN-LOAD CURVES FOR BIAXIAL COMPRESSION-TENSION

RATIO OF -1/0.052

Figure 7. Stress-strain curves for different stress ratios.

## 2.5 Pre- and post-processing of data

The use of a three dimensional formulation for structural analysis requires appropiate pre- and post-processing facilities. In pre-processing it is necessary to use mesh-generation programs to generate the geometry, element connectivity, boundary conditions and loading data from a very simple specification. In post-processing, plotting facilities for representation of deformed shapes and material state information should include the possibility of hidden line removal, different perspectives, rotation of the model, etc.

## 3. NUMERICAL EXAMPLES

Some examples are now presented to illustrate the performance of the 3D model.

### 3.1 Vecchio-Collins panels

Recently, Vecchio and Collins [8] conducted an excellent study on the behaviour of reinforced concrete panels under in-plane and normal stresses. In their experimental programme they tested 30 specimens of dimensions 890 x 890 x 70 mm. (see Figure 8) on a special testing rig which allowed a uniform plane stress state to be created in the panels. In all the cases the reinforcement was arranged parallel to the panel sides, but with different ratios and amounts for different specimens. Of the whole series, only two specimens will be considered here, namely panels number 27 and 25. Both have equal reinforcing ratios of 0.01785, in the x and y directions, so they were nominally identical, although the measured

Table 1 Material properties for the Vecchio-Collins panels

| | | | PANEL 27 | PANEL 25 |
|---|---|---|---|---|
| CONCRETE | | | | |
| Young's modulus, | $E_c$ | = | 20000. | 20000. KN/m$^2$ |
| Poisson's ratio, | $\nu$ | = | 0.15 | 0.15 |
| Ultimate compressive stress, | $f'_c$ | = | 20.5 | 19.3 KN/m$^2$ |
| Ultimate compressive strain, | $\varepsilon_{cu}$ | = | 0.0035 | 0.0035 |
| Cracking tensile stress, | $f'_t$ | = | 2.4 | 2.0 KN/m$^2$ |
| Fracture energy, | $G_f$ | = | 0.15 | 0.15 KN/m |
| shear reduction, | $k_1$ | = | 0.4 | 0.4 |
| strength reduction, | $k_2$ | = | 0.55 | 0.27 |
| elasticity limit, | $a_1$ | = | 0.3 | 0.3 |
| STEEL | | | | |
| Young's modulus, | $E_s$ | = | 200000. | 200000. KN/m$^2$ |
| Yield stress, | $f_y$ | = | 442. | 442. KN/m$^2$ |

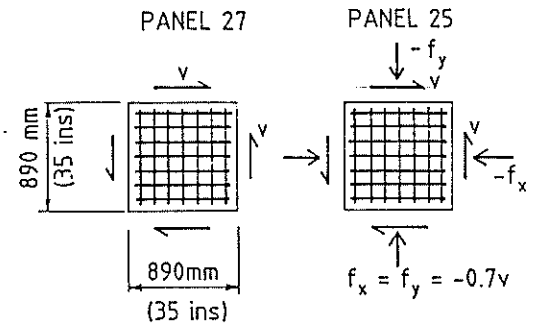


Thickness 70 mm (2.75 ins)

Figure 8. Vecchio-Collins panels. Geometry and loading.

Figure 9. Stress-strain curves for V-C panels.

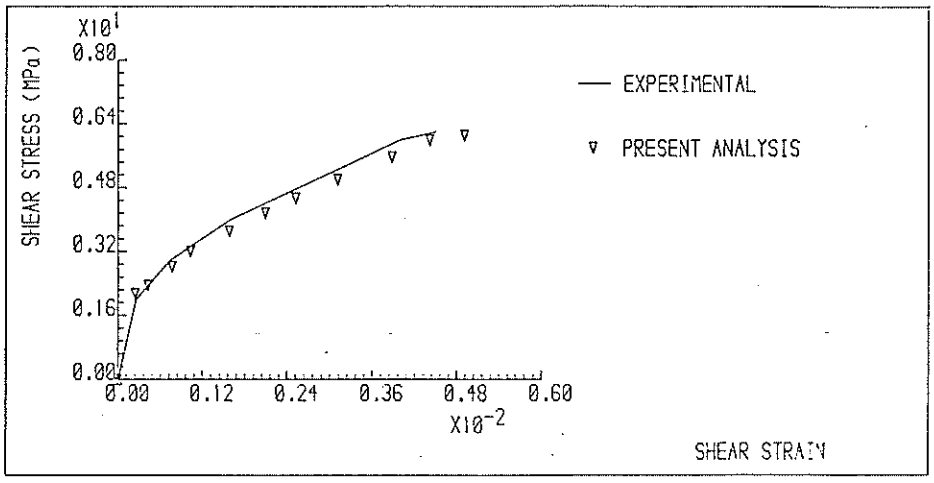


VECCHIO-COLLINS PANEL A

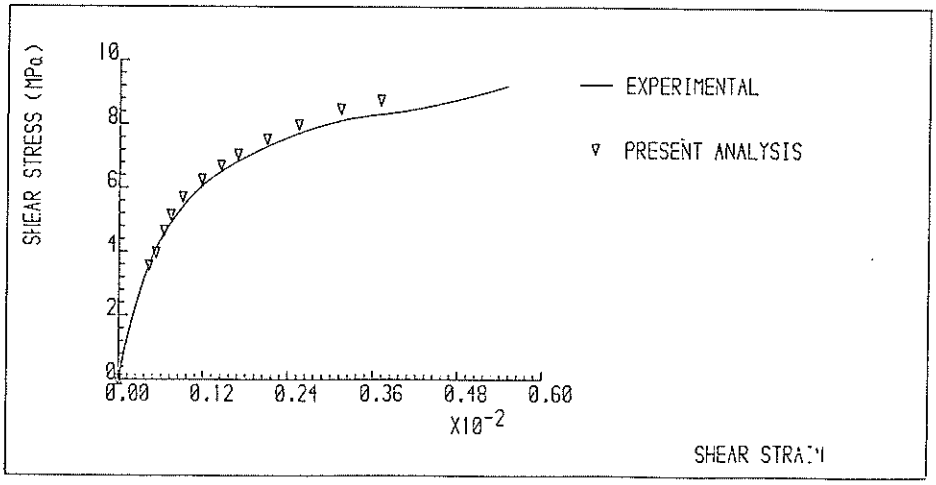


VECCHIO-COLLINS PANEL B

concrete properties were slightly different. The material properties used for the numerical analysis are shown in Table 1. Panel 27 was loaded in pure shear, while panel 25 was subjected to a combination of shear and biaxial compression (see Figure 8). Both panels were loaded proportionally.

The tests are designed so that the response of the panels is mainly dependent on the concrete behaviour. Both panels failed due to crushing of cracked concrete. These examples are included here because they are a demanding test on the computational material model. With one principal stress in tension and the other in compression the problem is designed to test both the tensile and compressive parts of the models, and their mutual influence. It is also interesting to observe how the additional biaxial compression in panel 25 influences the failure load in comparison with panel 27. Although a simple equilibrium analysis shows that the additional compression produces no change in the concrete stress, in reality, panel 25 showed a 44 per cent increase in the shear failure load.

The numerical analyses are performed using the initial stress method, with line search, and a tolerance of 1 per cent on the norm of the residual forces.

Results from the numerical analyses are shown in Figures 9(a) and 9(b). Excellent agreement between the experimental results and the numerical solution is obtained. Not only are the failure loads accurately predicted in both cases, but the complete stress-strain curves closely agree.

## 3.2 Analysis of deep beams

In this second example two deep beams experimentally studied by Ramakrishan and Anathanarayana [9] are analysed. Two

Table 2 Material properties for deep beams

| | | | 30 in. beam | 20 in. beam |
|---|---|---|---|---|
| CONCRETE | | | | |
| Young's modulus, | $E_c$ | = | 4600. | 4600. kips/in$^2$ |
| Poisson's ratio, | $\nu$ | = | 0.17 | 0.17 |
| Ultimate compressive stress, | $f'_c$ | = | 3.96 | 2.00 kips/in$^2$ |
| Ultimate compressive strain, | $\varepsilon_{cu}$ | = | 0.0035 | 0.0035 |
| Cracking tensile stress, | $f'_t$ | = | 0.36 | 0.23 kips/in$^2$ |
| Fracture energy, | $G_f$ | = | 0.0006 | 0.0006 kips/in |
| shear reduction, | $k_1$ | = | 0.5 | 0.5 |
| strength reduction, | $k_2$ | = | 0.5 | 0.5 |
| elasticity limit, | $\alpha_1$ | = | 0.3 | 0.3 |
| STEEL | | | | |
| Young's modulus, | $E_s$ | = | 29000. | 29000. kips/in$^2$ |
| Yield stress, | $f_y$ | = | 46. | 46. kips/in$^2$ |

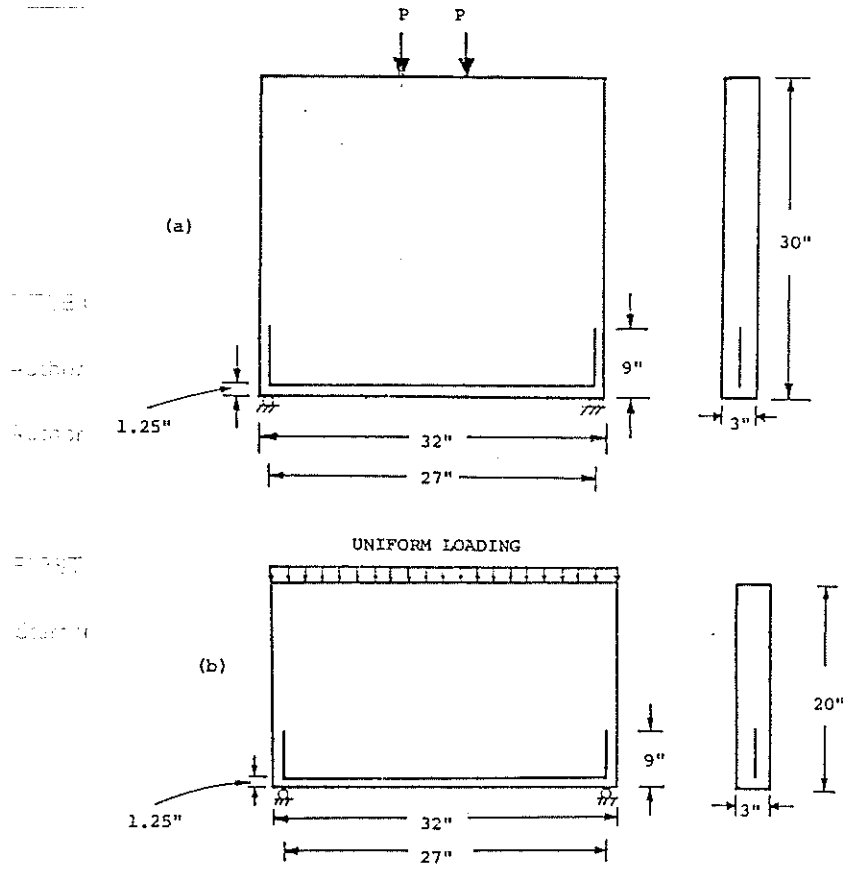


Figure 10. Deep beams. Geometry

beams are considered, one 30 in. and the other 20 in. deep. The first one is subjected to two point loads, while the other is loaded with a uniform pressure (see Figure 10). The reinforcement consists of one bar of cross section 1 in$^2$. The material properties used in the analysis are shown in Table 2.

By taking advantage of symmetry, only one half of the beams is discretised, using meshes of twenty solid elements.

The analyses are performed using the initial stress method with a tolerance of 1 per cent on the norm of the residual forces.

Load-deflection curves are shown in Figure 11. Excellent agreement with the experimental results is obtained. The ultimate loads are also accurately predicted.

The computed crack patterns at failure are shown in Figures 12(a) and 12(b). The experimentally observed cracks (a stable flexural crack at mid-span and an unstable one running

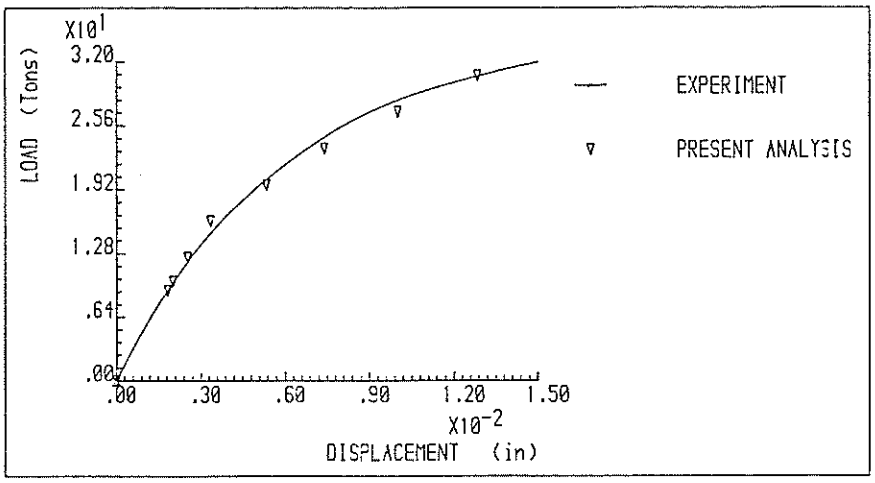


DISPLACEMENT-LOAD CURVE FOR 30 INCHES DEEP BEAM

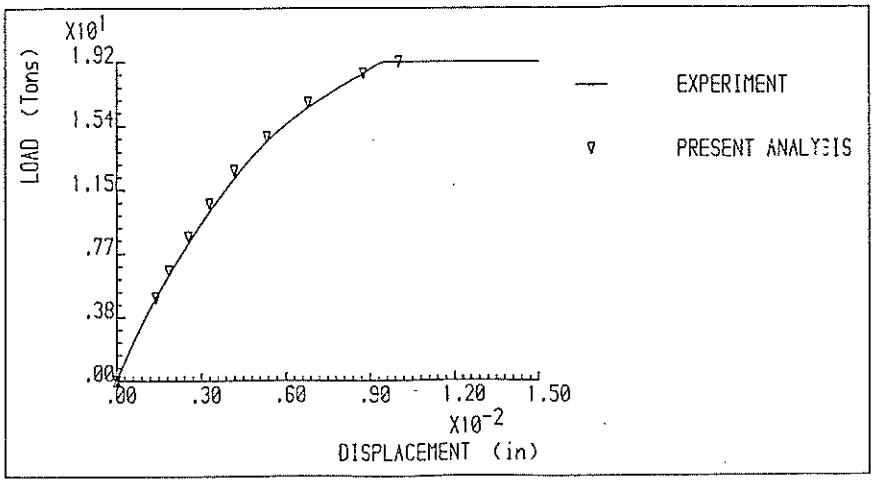


DISPLACEMENT-LOAD CURVE FOR 20 INCHES DEEP BEAM

Figure 11. Load-deflection curves for deep beams.

from the loads towards the support) are well predicted in the numerical analysis. Deformed shapes at failure are shown in Figure 13.

### 3.3 Illinois slab-column connection tests

Finally, two tests from a series carried out by Sunidja et al. [10] at the University of Illinois in Urbana-Champaign are studied. The object of these tests was to study the strength and behaviour of unbonded prestressed concrete plate-edge column connections representative of those used in prestressed flat plate buildings and subjected to static vertical loading.

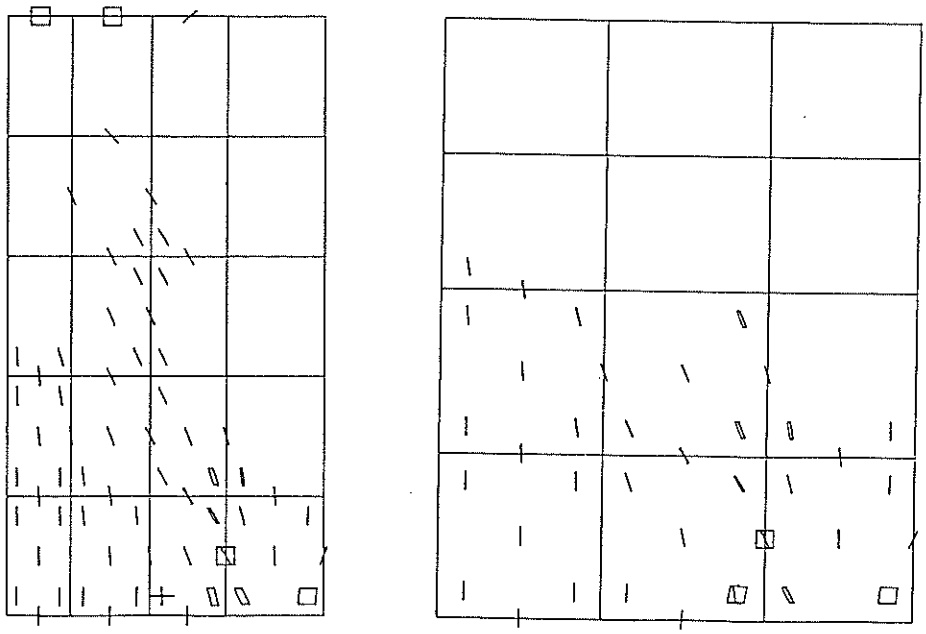

Figure 12. Crack patterns at failure for deep beams.

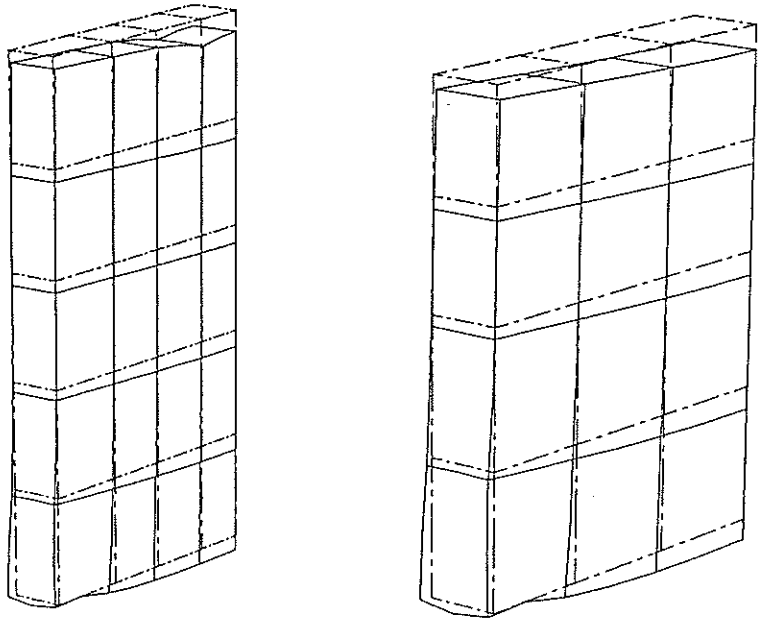

Figure 13. Deformed shapes at failure for deep beams.

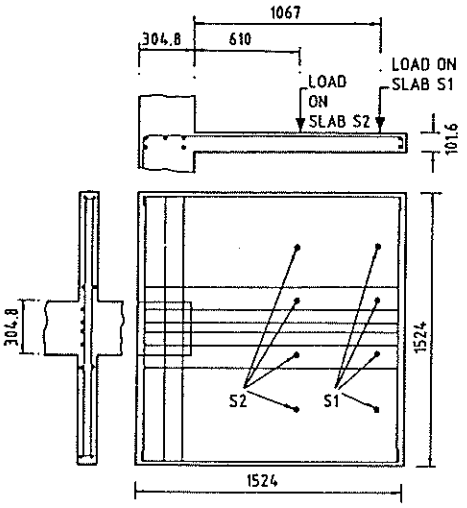


Figure 14. Illinois slab-column connections.Geometry and loading.

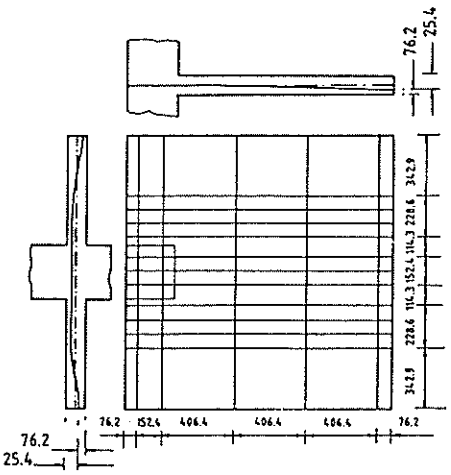


Figure 15. Arrangement of unbonded tendons.

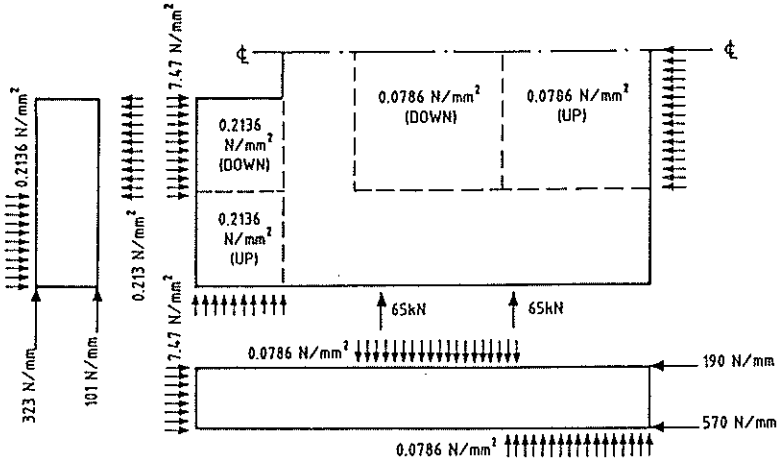


Figure 16. Load-pattern applied to model pre-tension forces.

The test specimens each consist of a 1524 mm. square pre- stressed concrete slab 101.6 mm. in total thickness and with a 304.8 mm. square column located adjacent to and centered along one edge of the slab. The system and the dimensions of the slab are shown in Figure 14.

The two-way flat slabs are prestressed in both directions. The arrangement of the tendons is shown in Figure 15. In addition, No. 3 deformed bars (71 mm² cross-sectional area) are used as bonded reinforcement as shown in Figure 14.

The slabs are loaded by four concentrated loads placed at a distance of 1066.8 mm. from the column face for slab S1 and 609.6 mm. for slab S2.

By taking advantage of symmetry only one half of the slab is discretized in each analysis. The slabs are assumed to be clamped at the column edge. This assumption is justified because the heavily reinforced column is very stiff when compared to the slab.

The pre-tension forces are represented by a horizontal load at the slab edges. To account for the pretension forces due to the curvature of the tendons additional lateral forces are applied to the slabs, as shown in Figure 16. In the analysis the pre-tension and the self-weight load of 25000 N/mm³ are applied as initial loads and kept constant during the incrementation of the concentrated loads.

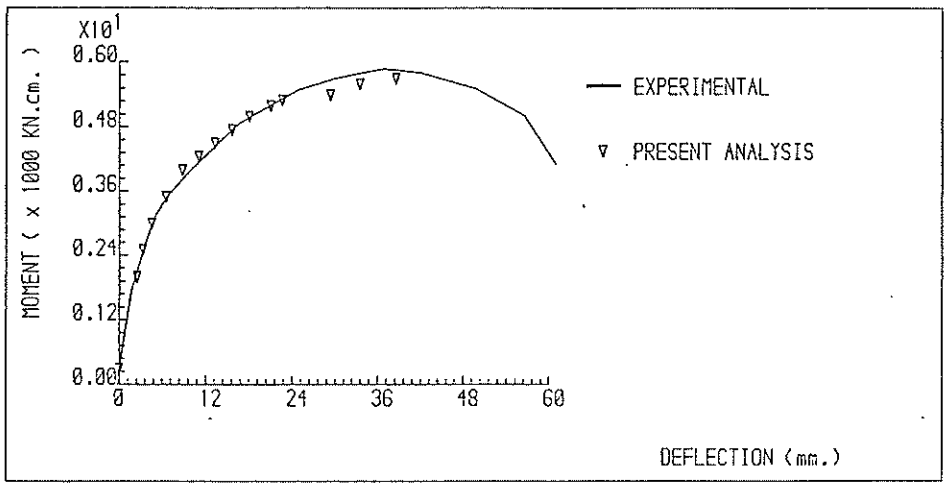


LOAD-DEFLECTION CURVE FO ILLINOIS SLAB S1

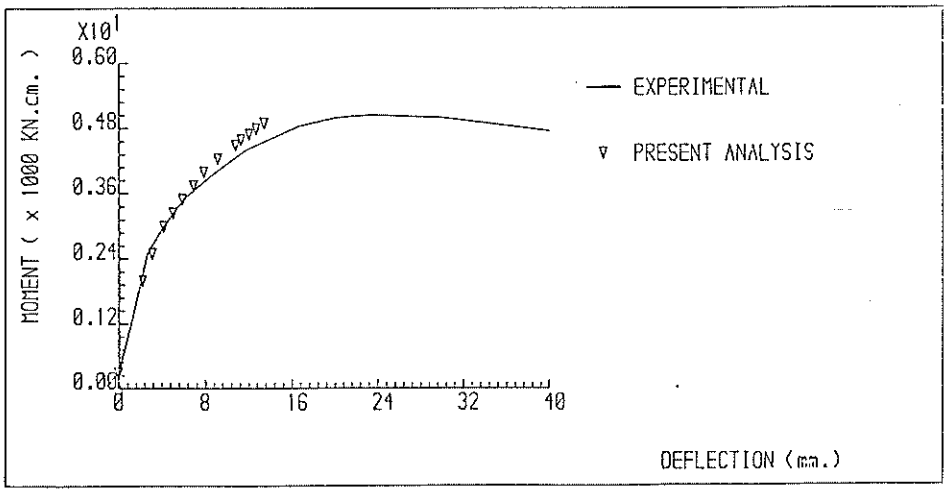


LOAD-DEFLECTION CURVE FOR ILLINOIS SLAB S2

Figure 17. Load-deflection curves for Illinois slabs.

Table 3 Material properties for the Illinois slab-column

| | | | S1 | S2 | |
|---|---|---|---|---|---|
| CONCRETE | | | | | |
| Young's modulus, | $E_c$ | = | 29000. | 24000. | N/mm$^2$ |
| Poisson's ratio, | $\nu$ | = | 0.15 | 0.15 | |
| Ultimate compressive stress, | $f'_c$ | = | 50.0 | 43.0 | N/mm$^2$ |
| Ultimate compressive strain, | $\varepsilon_{cu}$ | = | 0.0035 | 0.0035 | |
| Cracking tensile stress, | $f'_t$ | = | 3.67 | 3.15 | N/mm$^2$ |
| Fracture energy, | $G_f$ | = | 0.10 | 0.10 | N/mm |
| shear reduction, | $k_1$ | = | 0.50 | 0.50 | |
| strength reduction, | $k_2$ | = | 0.50 | 0.50 | |
| elasticity limit, | $\alpha_1$ | = | 0.30 | 0.30 | |
| STEEL | | | | | |
| Young's modulus, | $E_s$ | = | 200000. | 200000. | N/mm$^2$ |
| Yield stress, | $f_y$ | = | 500. | 500. | N/mm$^2$ |

Both analyses are performed using the KT1 method with line search. A tolerance of 1 per cent on the norm of the residual forces is adopted.

The meshes used for the analyses can be seen in Figures 18 and 19, respectively. Both meshes consist of twenty, 20-node elements.

The material properties used for the analyses are summarized in Table 3.

In Figure 17 the moment-deflection relations obtained from the numerical computations are compared with the test results. The moment is obtained by multiplying the total applied load by the distance from the load to the face of the column. The initial moment caused by the self-weight of the slab is 288 KN.cm. The deflections shown are the additional values due to the concentrated loads and do not include the deformation caused by either the dead load or the pre-tension. The deflection is measured at the east edge of the slab, and on the axis of symmetry.

In the experiment, slab S1 failed in a flexural mode, while slab S2 collapsed due to a dominant shear crack. Figure 17(a) shows that both the initial stiffness and the progressively nonlinear response of slab S1 are accurately predicted by the analysis. The failure load is very well predicted. Results for slab S2 , shown in Figure 17(b), are also in close agreement with the experiment, although a slightly less ductile behaviour at failure than in the experiment is observed.

Figures 18 and 19 show the spread of the cracking on the tension side of the slabs (top surfaces) for different load levels. As expected, cracking is mostly confined to the part

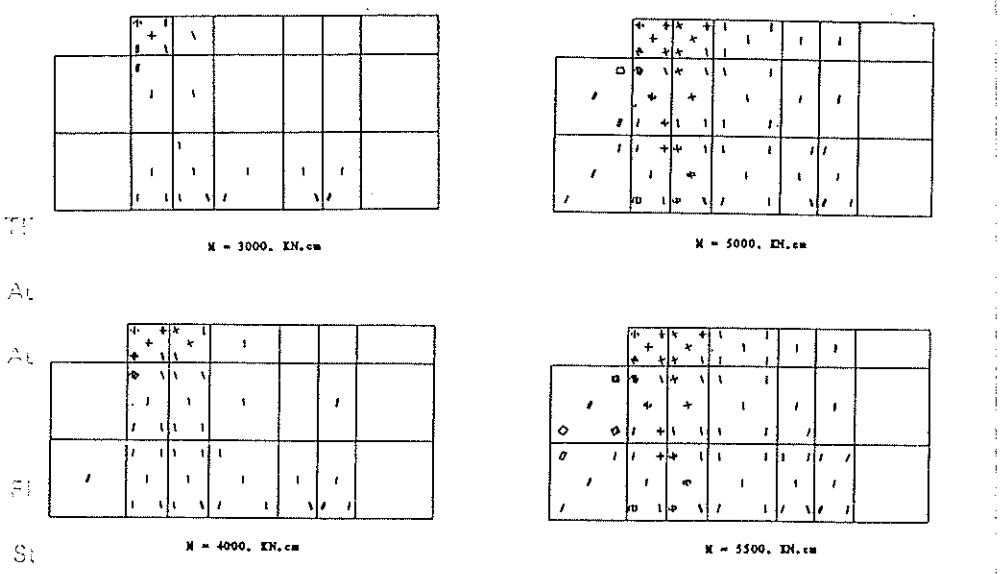


Figure 18. Crack patterns for slab S1 at different load levels.

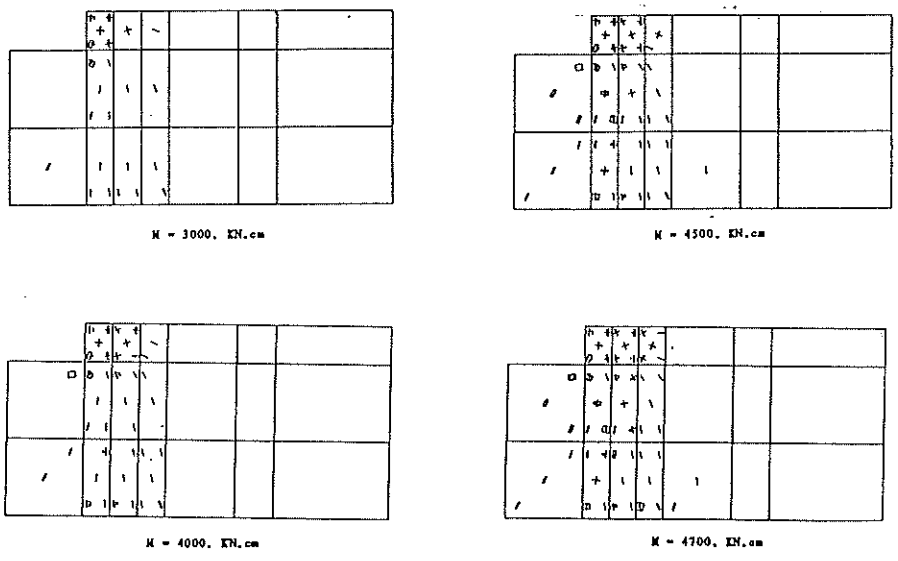


Figure 19. Crack patterns for slab S2 at different load levels.

of the slabs between the support and the location of the loads. In both cases, cracks start to form close to the column, where tensile stresses are larger, and gradually spread towards the loads and through the thickness. Some double-cracking is observed around the column in both cases.

## 4. REFERENCES

1. ZIENKIEWICZ, O.C., GAGO, J.P.S.R. and KELLY, D.W. - 'The hierarchical concept in finite element analysis'. Computres ans Structures, 1984, 16, 1-4.

2. IRONS, B.M. - 'Quadrature rules for brick based finite elements'. IJNME, 1971, 3, 293-294.

3. OWEN, D.R.J. and FIGUEIRAS, J.A. - 'Ultimate load analysis of reinforced concrete plates and shells including geometric nonlinear effects', Finite element software for plates and shells, Ed. Hinton, E. and Owen, D.R.J., Pineridge Press, 1984.

4. KUPFER, H., HILSDORF, K.H. and RUSH, H. - 'Behaviour of concrete under biaxial stress'. ACI Journal, 1969, 66, 656-666.

5. GLEMBERG, R. - Dynamic analysis of concrete structures, Dept. of Struc. Mech., Chalmers University of Technology, Pub. 84:1, 1984.

6. CERVENKA, V. - 'Constitutive model for cracked reinforced concrete'. ACI Journal, 1985, 82, 877-882

7. CERVERA, M. - Nonlinear analysis of reinforced concrete structures using three dimensional and shell finite element models. Ph. D. Thesis, University of Wales, Swansea, 1986 (subm.)

8. VECCHIO, F. and COLLINS, M.P. - The response of reinforced concrete to in-plane shear and normal stresses. Pub. 82-03, Dept. of Civil Engng, Univ. of Toronto, 1982.

9. RAMAKRISHAN, V. and ANATHANARAYANA, Y. - 'Ultimate strength of deep beams in shear'. ACI Journal, 1968, 65, 87-98.

10. SUNIDJA, H., FOUTCH, D.A. and GAMBLE, W.L. - Response of prestressed concrete plate-edge column connections. Civil Engng. Studies, Structural Research Series, 498, Univ. of Illinois, Urbana-Champaign, 1982.